

Theory and Neutrons Combine to Reveal A Family of Layered Perovskites Without Inversion Symmetry

Tong Zhu, Toby Cohen, Alexandra S. Gibbs, Weiguo Zhang, P. Shiv Halasyamani, Michael A. Hayward* and Nicole A. Benedek*

Supporting Information

1. Structural characterization of CsNdTa₂O₇, RbNdNb₂O₇ and RbNdTa₂O₇ using synchrotron X-ray powder diffraction data vs. neutron powder diffraction data.

Table S1. Fitting statistics from the structural refinement of CsNdTa₂O₇ against synchrotron X-ray and neutron powder diffraction data.

Table S2. Fitting statistics from the structural refinement of RbNdNb₂O₇ against synchrotron X-ray and neutron powder diffraction data.

Table S3. Fitting statistics from the structural refinement of RbNdTa₂O₇ against synchrotron X-ray and neutron powder diffraction data.

Figure S1. Observed calculated and difference plots from the structural refinement of CsNdTa₂O₇ against Synchrotron X-ray powder diffraction data. Top and middle plots show fits using a *P2₁am* model. For comparison the bottom plot shows a fit using an *I2cm* model. Arrows indicate weak peaks in the data (solid) or in the model (dashed) which indicate the *I2cm* model is incorrect.

Figure S2. Observed calculated and difference plots from the structural refinement of RbNdTa₂O₇ against Synchrotron X-ray powder diffraction data. Top and middle-left plots show fits using an *I2cm* model. For comparison the middle-right plot shows a fit using an *Imam* model bottom and the bottom plot shows a fit using a *P2₁am* model. Arrows indicate weak peaks in the data (solid) or in the model (dashed) which indicate the *P2₁am* model is incorrect.

Figure S3. Observed calculated and difference plots from the refinement, against neutron powder diffraction data collected from CsNdTa₂O₇, of structural models in space group *P2₁am*, *Imam* and *I2cm*. Panels on the right show expanded plots in the region $1.2 < d/\text{\AA} < 1.8$ highlighting the difference in the quality of the fits with the different models.

Figure S4. Observed calculated and difference plots from the refinement, against neutron powder diffraction data collected from RbNdNb₂O₇, of structural models in space group *P2₁am*, *Imam* and *I2cm*. Panels on the right show expanded plots in the region $1.2 < d/\text{\AA} < 1.8$ highlighting the difference in the quality of the fits with the different models.

Figure S5. Observed calculated and difference plots from the refinement, against neutron powder diffraction data collected from RbNdTa₂O₇, of structural models in space group *P2₁am*, *Imam* and *I2cm*, plotted as a function of d-spacing (\AA). Panel on the right show expanded plots in the region $1.2 < d/\text{\AA} < 1.8$ highlighting the difference in the quality of the fits with the different models.

2. Particle-size dependent second-harmonic response.

Figure S6. Plot of SHG activity of CsNdTa₂O₇ as a function of particle size, compared to KH₂PO₄ (KDP) standard.

Figure S7. Plot of SHG activity of RbNdTa₂O₇ as a function of particle size, compared to KH₂PO₄ (KDP) standard.

3. Refined structural data

Figure S8. Observed, calculated and difference plots from the refinement of a structural model in space group *I2cm* (#46) against neutron powder diffraction data collected from RbNdNb₂O₇ at 298 K ($\chi^2 = 8.23$). Top panel shows data from the 168° detector bank, bottom panel from the 90° detector bank.

Figure S9. Observed, calculated and difference plots from the refinement of a structural model in space group *P2₁am* (#26) against neutron powder diffraction data collected from CsNdTa₂O₇ at 298 K ($\chi^2 = 5.63$). Top panel shows data from the 168° detector bank, bottom panel from the 90° detector bank.

Figure S10. Observed, calculated and difference plots from the refinement of a structural model in space group *I2cm* (#46) against neutron powder diffraction data collected from RbNdTa₂O₇ at 298 K. Top panel shows data from the 168° detector bank, bottom panel from the 90° detector bank.

Table S4. Parameters from the structural refinement of RbNdNb₂O₇ against neutron powder diffraction data collected at 298 K.

Table S5. Parameters from the structural refinement of CsNdTa₂O₇ against neutron powder diffraction data collected at 298 K.

Table S6. Parameters from the structural refinement of RbNdTa₂O₇ against neutron powder diffraction data collected at 298 K.

Table S7. Selected bond lengths from the refined structure of RbNdNb₂O₇

Table S8. Selected bond lengths from the refined structure of CsNdTa₂O₇

Table S9. Selected bond lengths from the refined structure of RbNdTa₂O₇

1. Structural characterization of CsNdTa₂O₇, RbNdNb₂O₇ and RbNdTa₂O₇ using synchrotron X-ray powder diffraction data vs. neutron powder diffraction data.

Three structural models, each describing a different distorted $n = 2$ Dion-Jacobson structure, were refined against synchrotron X-ray powder diffraction data collected from CsNdTa₂O₇, RbNdNb₂O₇ and RbNdTa₂O₇. Specifically models in space groups $P2_1am$ (#26), $Imam$ (#74) and $I2cm$ (#46) which describe $a^-a^-c^+$, $a^-a^-c^0/-(a^-a^-c^0)$ and $a^-a^-c^+/-(a^-a^-c^+)$ distortions respectively, were refined against the data to give the fitting statistics shown in Tables S1-S3.

	Synchrotron X-ray				Neutron			
Space group	χ^2	wRp (%)	Rp (%)	number of variables	χ^2	wRp (%)	Rp (%)	number of variables
$P2_1am$ (#26)	4.29	3.06	1.84	51	5.63	4.80	5.21	61
$Imam$ (#74)	4.36	3.10	1.89	43	48.74	14.11	11.75	53
$I2cm$ (#46)	4.33	3.07	1.87	51	47.53	13.95	11.43	61

Table S1. Fitting statistics from the structural refinement of CsNdTa₂O₇ against synchrotron X-ray and neutron powder diffraction data.

	Synchrotron X-ray				Neutron			
Space group	χ^2	wRp (%)	Rp (%)	number of variables	χ^2	wRp (%)	Rp (%)	number of variables
$P2_1am$ (#26)	5.05	5.79	3.81	51	103.10	16.31	12.12	61
$Imam$ (#74)	5.12	5.85	3.84	43	68.07	13.22	11.10	53
$I2cm$ (#46)	4.97	5.76	3.78	51	8.23	6.31	6.25	61

Table S2. Fitting statistics from the structural refinement of RbNdNb₂O₇ against synchrotron X-ray and neutron powder diffraction data.

	Synchrotron X-ray				Neutron			
Space group	χ^2	wRp (%)	Rp (%)	number of variables	χ^2	wRp (%)	Rp (%)	number of variables
$P2_1am$ (#26)	6.81	3.78	2.33	51	86.69	15.63	11.63	61
$Imam$ (#74)	6.87	3.81	2.36	43	40.59	10.70	9.56	53
$I2cm$ (#46)	6.76	3.75	2.31	51	8.33	4.85	4.96	61

Table S3. Fitting statistics from the structural refinement of RbNdTa₂O₇ against synchrotron X-ray and neutron powder diffraction data.

Considering the fitting statistics from the refinements against the synchrotron X-ray powder diffraction data, it is impossible to state with any confidence which is the correct structure. While the $P2_1am$ model achieves the best statistical fit for CsNdTa₂O₇ and the $I2cm$ for RbNdNb₂O₇ and RbNdTa₂O₇, the margin of ‘victory’ is too small to be confident that these are the correct structures.

X-ray powder diffraction data are relatively insensitive to the distortions of Dion-Jacobson phases because the largest deformation of the lattice arises from the displacement of light oxide ions, which have small X-ray scattering cross sections. As a result the additional peaks observed in diffraction data, as the symmetry of the system is lowered from that of the $P4/mmm$ aristotype, are extremely weak. Figure S1 shows fits to the synchrotron X-ray

powder diffraction data collected from CsNdTa₂O₇ using a *P2₁am* model (shown to be correct by neutron powder diffraction) and an *I2cm* model. It can be seen that the *P2₁am* model accounts for a series of weak peaks that the *I2cm* model does not, however the intensity of these ‘additional’ diffraction peaks is much less than 1% of the most intense peak in the pattern, so that while it is in principle possible to exclude the *I2cm* model using these data, the fitting statistics of refinements using the two models are very similar. Furthermore, given the weakness of the ‘additional’ diffraction peaks, it is not possible to accurately quantify the magnitude of the oxide ion displacements, as the only information about the size of these displacements comes from the relative intensity of the ‘additional’ peaks which is hard to measure accurately, even with synchrotron radiation.

Figure S2 shows analogous fits to the synchrotron X-ray powder diffraction data collected from RbNdTa₂O₇ using an *I2cm* model (shown to be correct by neutron powder diffraction), an *Imam* model and a *P2₁am* model. Again it can be seen that the features which differentiate between the two models are extremely weak. In addition, because the space groups *I2cm* and *Imam* have the same extinction conditions, it can be seen that the only way to differentiate between the *I2cm* and *Imam* models is by the relative intensity of the extremely weak ‘additional’ diffraction peaks, resulting in similar fitting statistics for refinements using these two models. Thus we can conclude that it is extremely difficult to accurately determine the symmetry and magnitude of the structural distortions of Dion-Jacobson phases from X-ray powder diffraction data alone.

In contrast, high-resolution neutron powder diffraction data are much more sensitive to the distortions of these phases. Tables S1-S3 list the fitting statistics for refinements using the *P2₁am*, *Imam* and *I2cm* models against neutron powder diffraction data collected from CsNdTa₂O₇, RbNdNb₂O₇ and RbNdTa₂O₇. It can be seen in each case one model (*P2₁am* for CsNdTa₂O₇ and *I2cm* for RbNdNb₂O₇ and RbNdTa₂O₇) is far superior to the other two. This is because the displacement of oxide ions leads to much larger changes in the observed diffraction data. This can be seen in Figures S3-S5 which show comparative fits for each of the three structural models (*P2₁am*, *Imam* and *I2cm*) to the neutron diffraction data collected from each of the three samples. These data clearly and unambiguously show that CsNdTa₂O₇ adopts a *P2₁am*-type distortion while RbNdNb₂O₇ and RbNdTa₂O₇ adopt *I2cm*-type distortions.

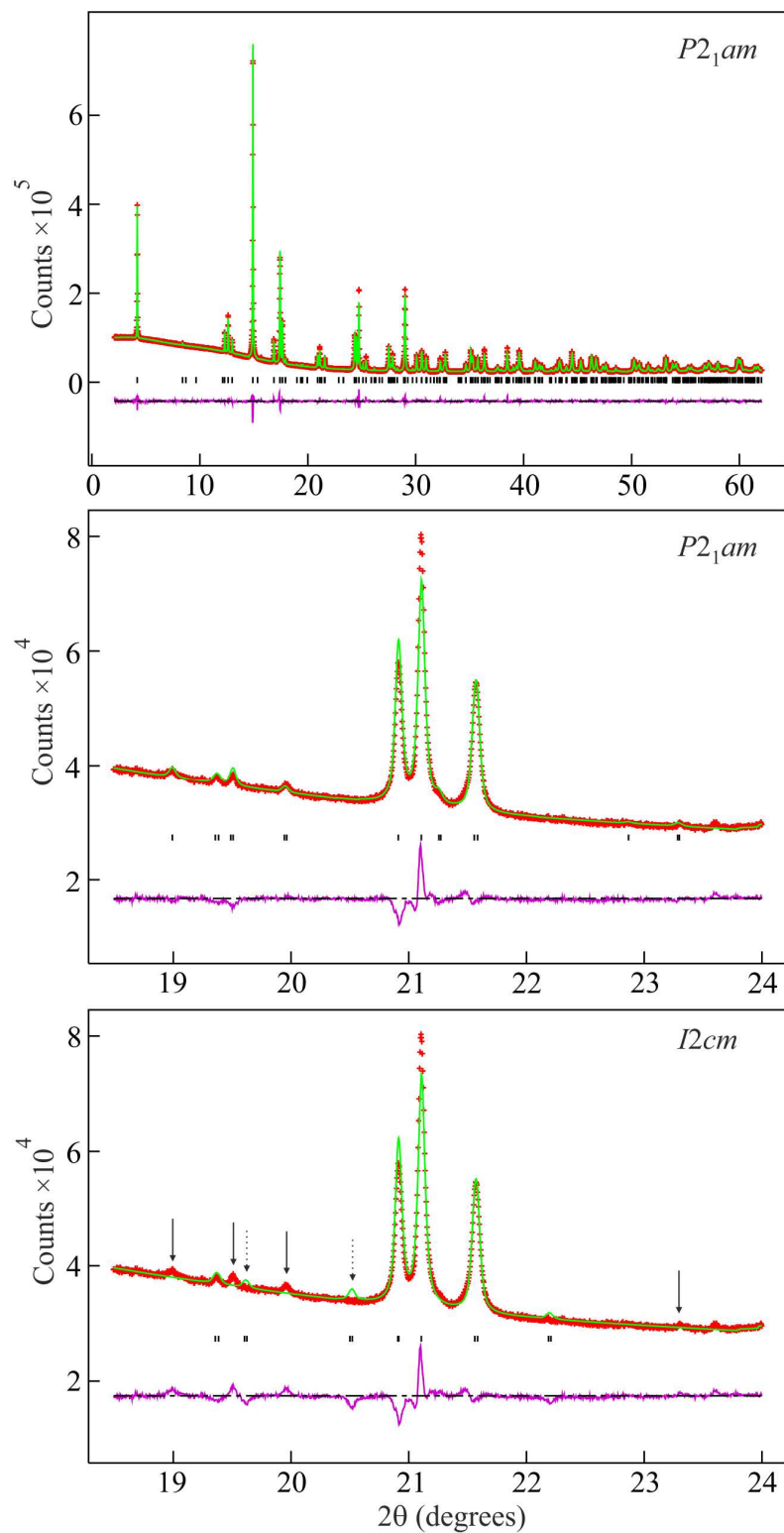


Figure S1. Observed calculated and difference plots from the structural refinement of $\text{CsNdTa}_2\text{O}_7$ against Synchrotron X-ray powder diffraction data. Top and middle plots show fits using a $P2_1am$ model. For comparison the bottom plot shows a fit using an $I2cm$ model. Arrows indicate weak peaks in the data (solid) or in the model (dashed) which indicate the $I2cm$ model is incorrect.

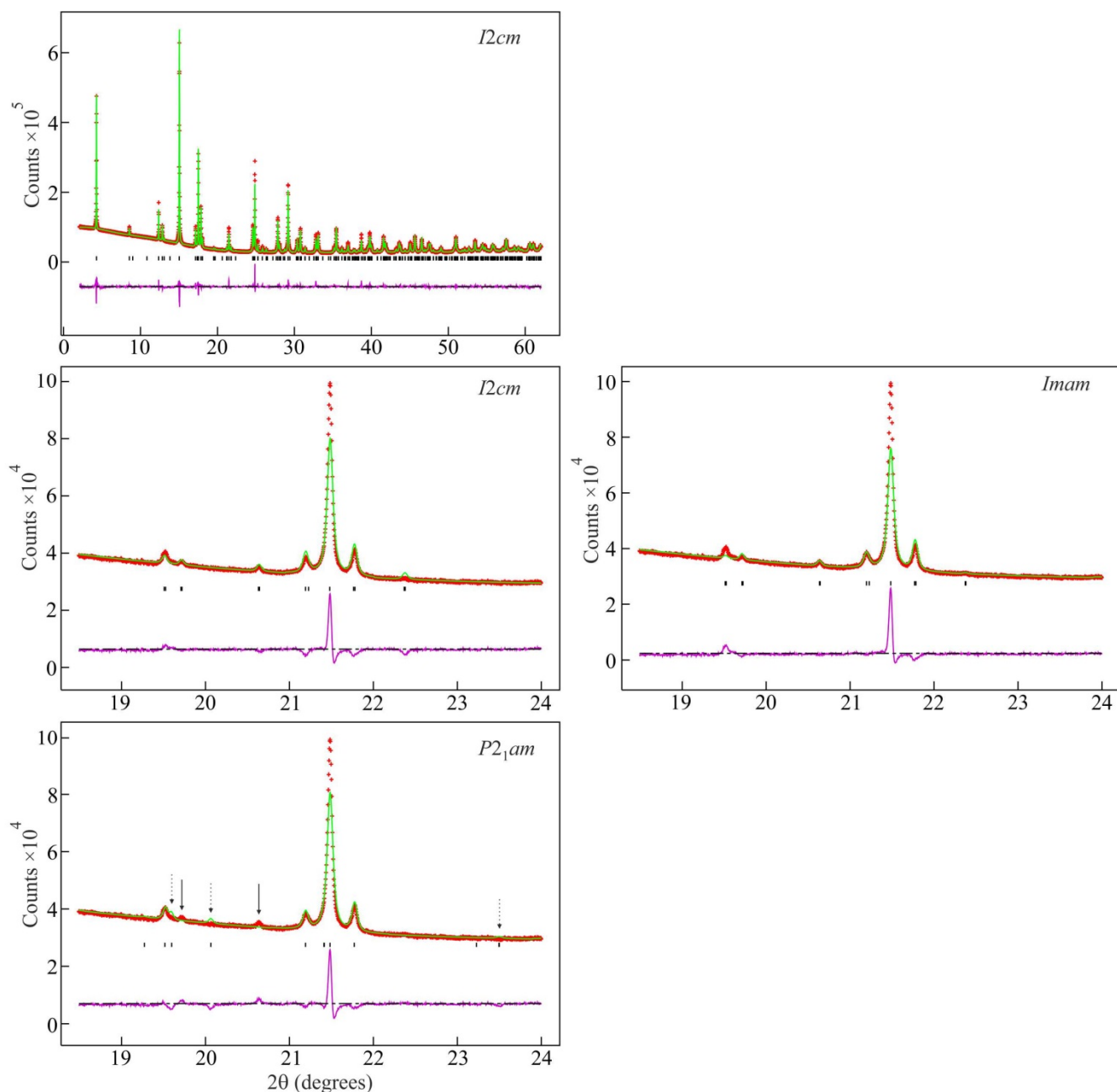


Figure S2. Observed calculated and difference plots from the structural refinement of $\text{RbNdTa}_2\text{O}_7$ against Synchrotron X-ray powder diffraction data. Top and middle-left plots show fits using an $I2cm$ model. For comparison the middle-right plot shows a fit using an $Imam$ model bottom and the bottom plot shows a fit using a $P2_1am$ model. Arrows indicate weak peaks in the data (solid) or in the model (dashed) which indicate the $P2_1am$ model is incorrect.

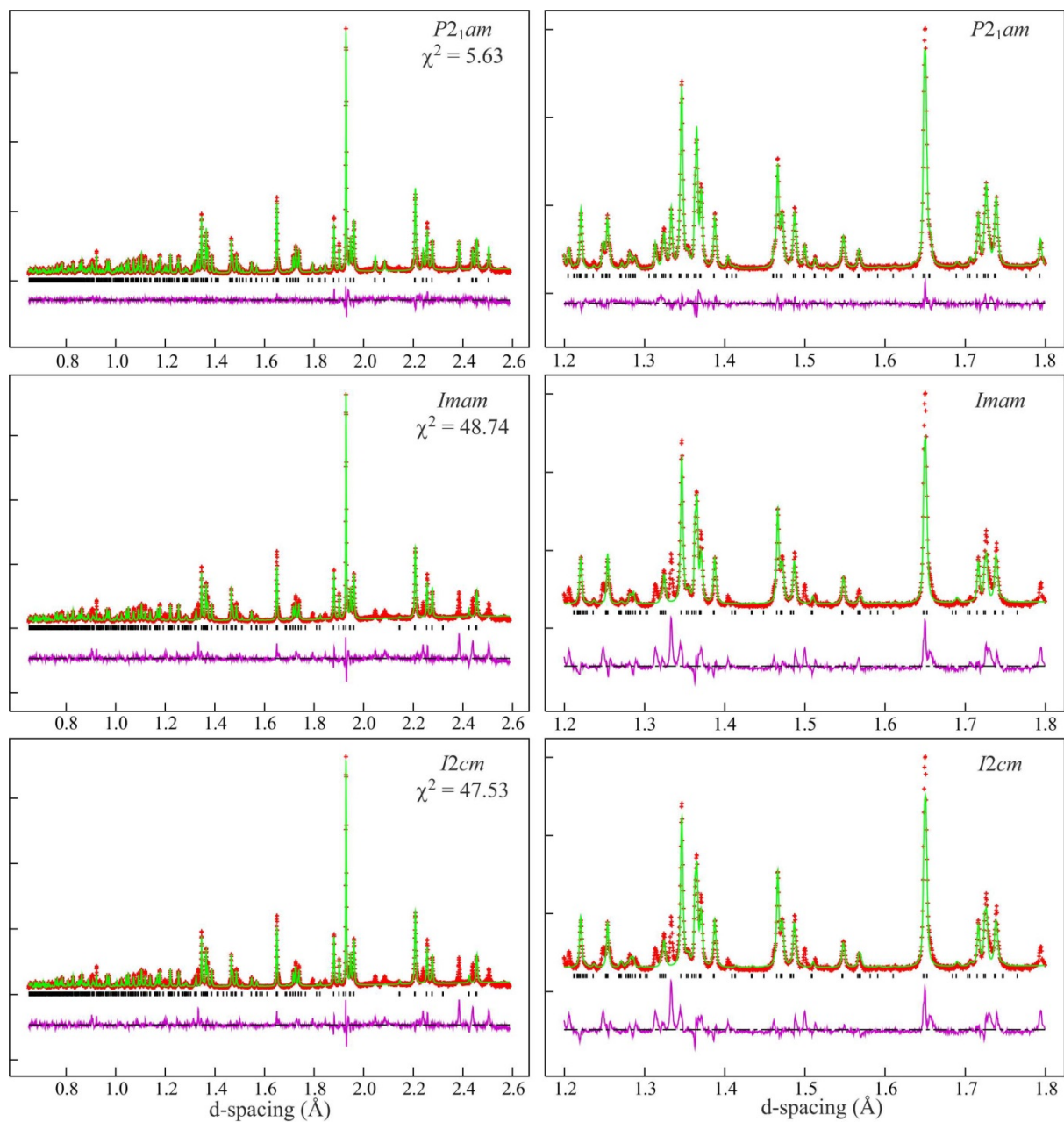


Figure S3. Observed calculated and difference plots from the refinement, against neutron powder diffraction data collected from $\text{CsNdTa}_2\text{O}_7$, of structural models in space group $P2_1am$, $Imam$ and $I2cm$. Panels on the right show expanded plots in the region $1.2 < d/\text{\AA} < 1.8$ highlighting the difference in the quality of the fits with the different models.

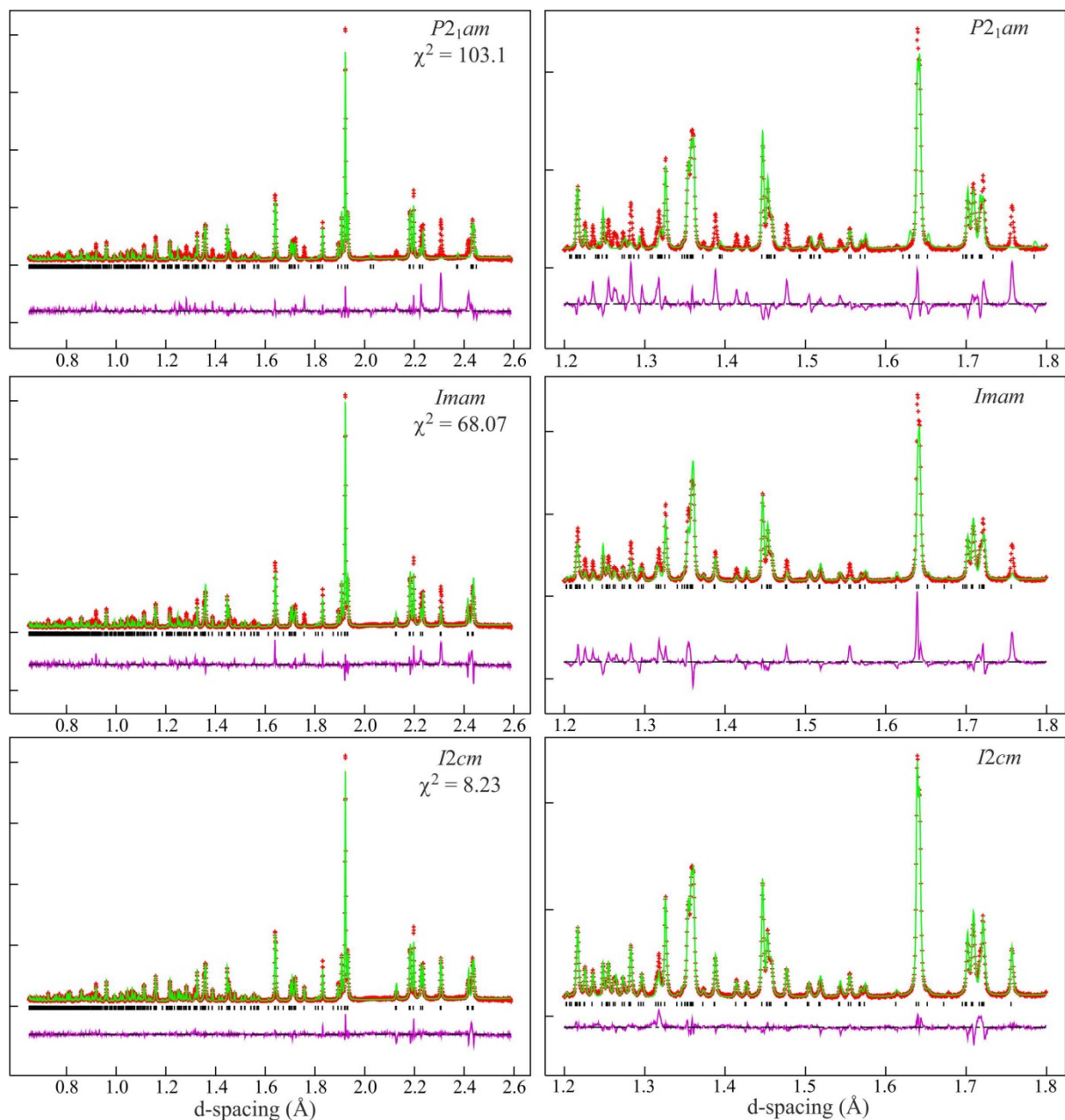


Figure S4. Observed calculated and difference plots from the refinement, against neutron powder diffraction data collected from $\text{RbNdNb}_2\text{O}_7$, of structural models in space group $P2_1am$, $Imam$ and $I2cm$. Panels on the right show expanded plots in the region $1.2 < d/\text{\AA} < 1.8$ highlighting the difference in the quality of the fits with the different models.

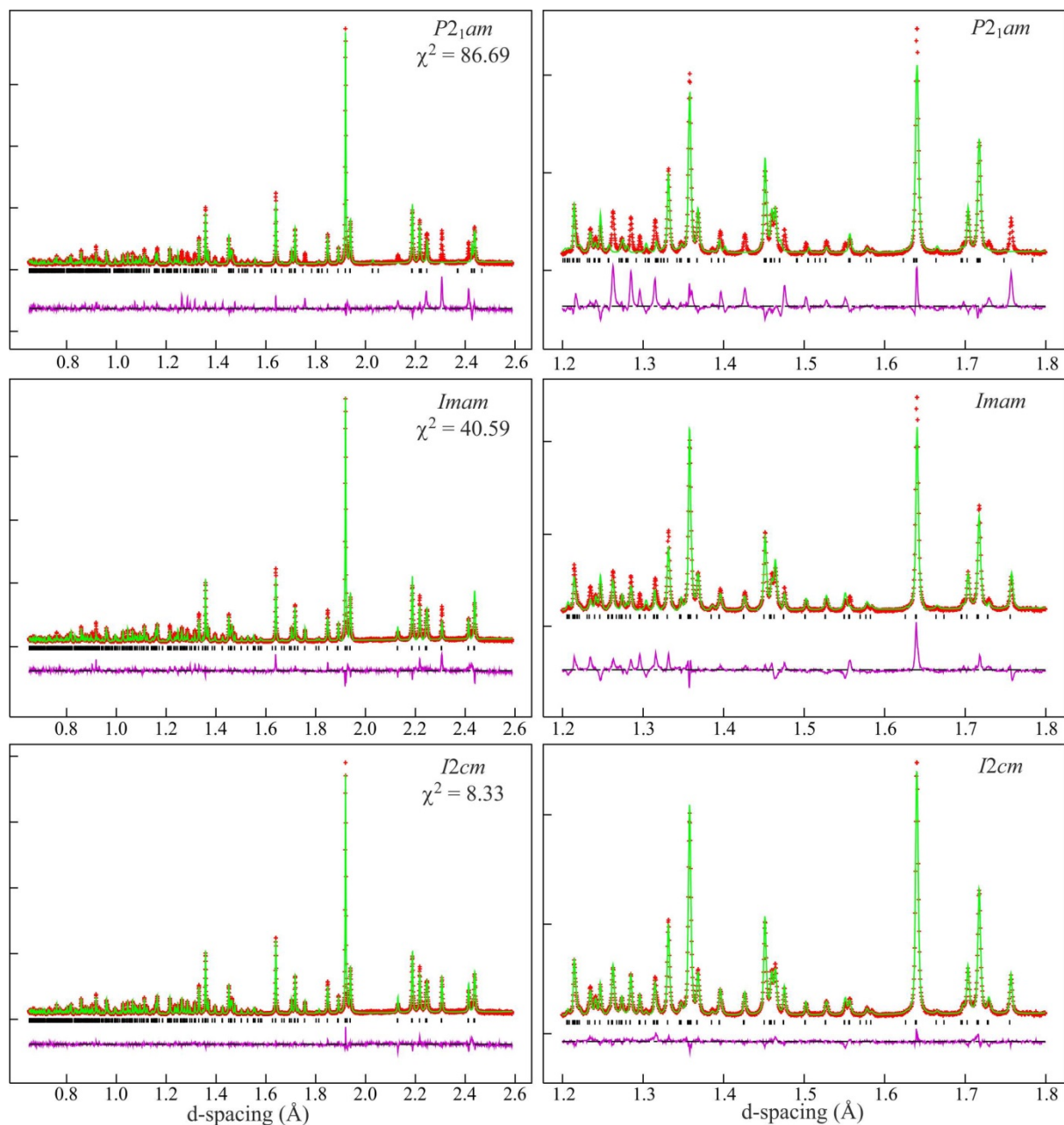


Figure S5. Observed calculated and difference plots from the refinement, against neutron powder diffraction data collected from $\text{RbNdTa}_2\text{O}_7$, of structural models in space group $P2_1am$, $Imam$ and $I2cm$, plotted as a function of d-spacing (\AA). Panel on the right show expanded plots in the region $1.2 < d/\text{\AA} < 1.8$ highlighting the difference in the quality of the fits with the different models.

2. Particle-size dependent second-harmonic response

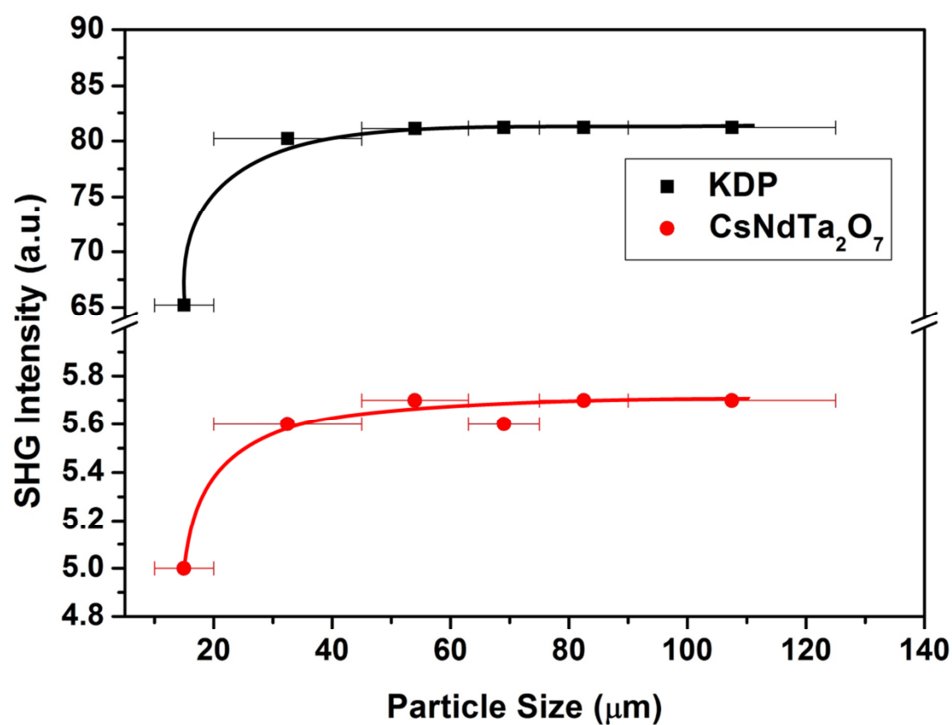


Figure S6. Plot of SHG activity of $\text{CsNdTa}_2\text{O}_7$ as a function of particle size, compared to KH_2PO_4 (KDP) standard.

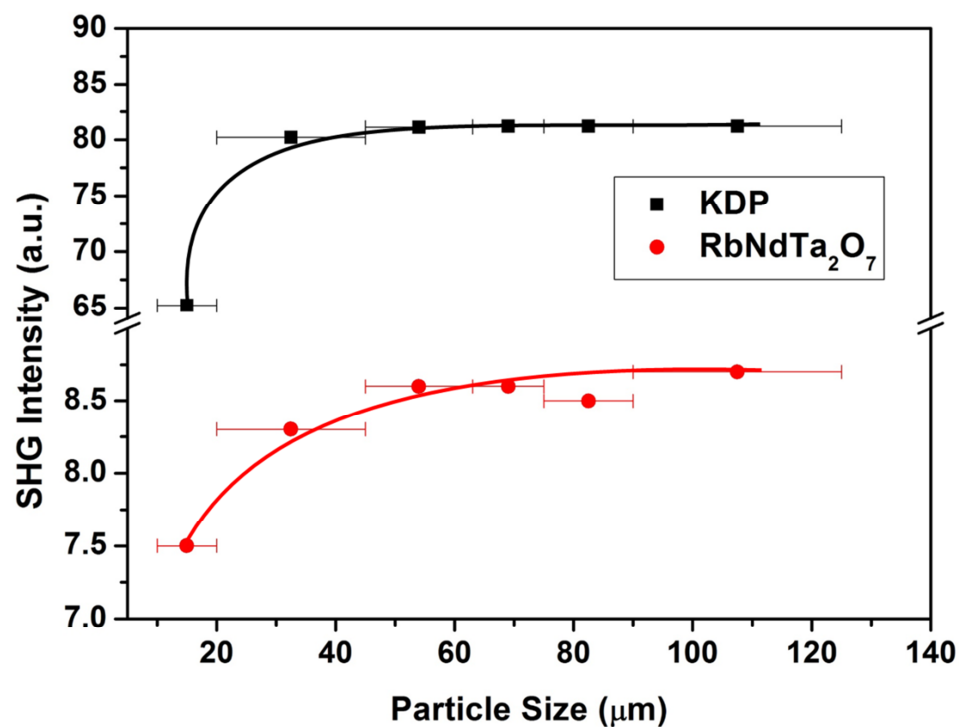


Figure S7. Plot of SHG activity of $\text{RbNdTa}_2\text{O}_7$ as a function of particle size, compared to KH_2PO_4 (KDP) standard.

3. Refined structural data

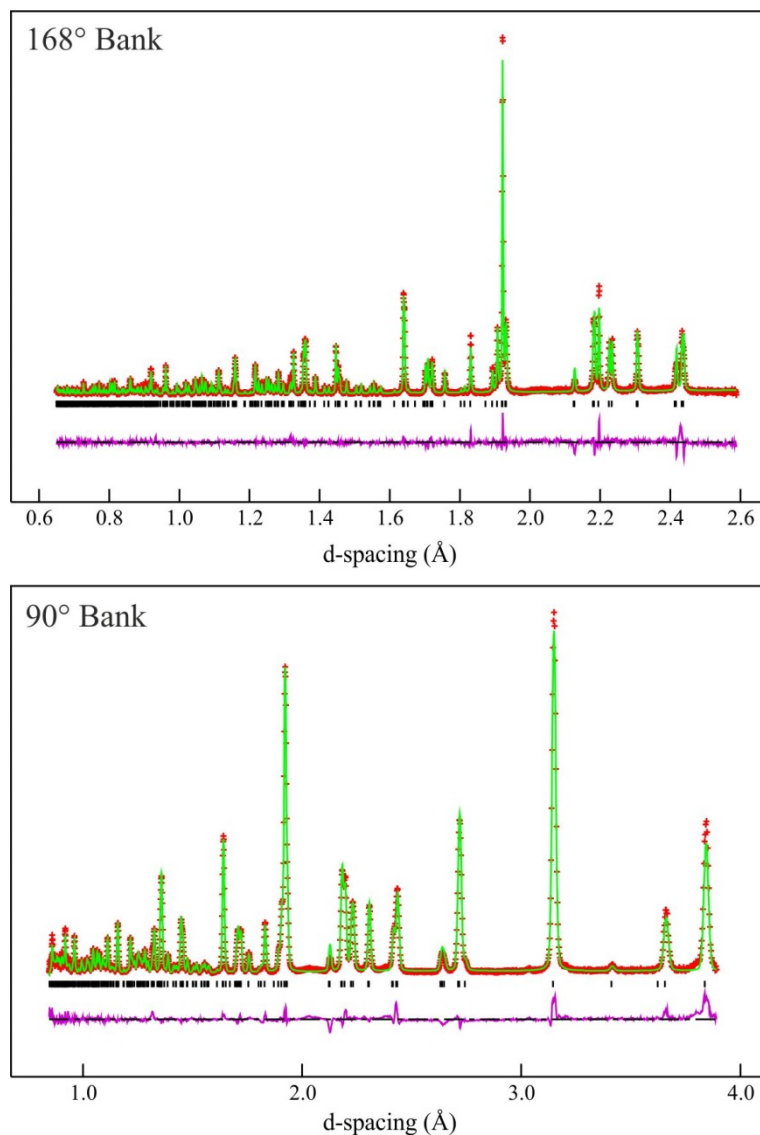


Figure S8. Observed, calculated and difference plots from the refinement of a structural model in space group $I2cm$ (#46) against neutron powder diffraction data collected from $\text{RbNdNb}_2\text{O}_7$ at 298 K ($\chi^2 = 8.23$). Top panel shows data from the 168° detector bank, bottom panel from the 90° detector bank.

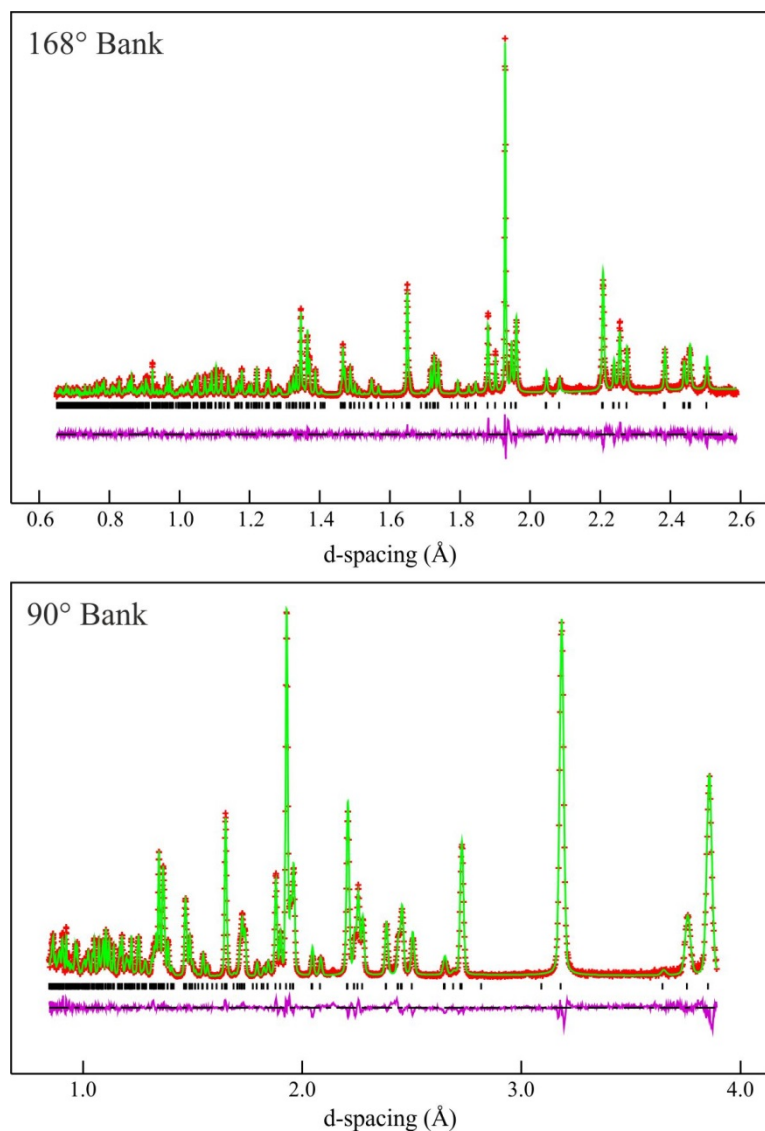


Figure S9. Observed, calculated and difference plots from the refinement of a structural model in space group $P2_1am$ (#26) against neutron powder diffraction data collected from $\text{CsNdTa}_2\text{O}_7$ at 298 K ($\chi^2 = 5.63$). Top panel shows data from the 168° detector bank, bottom panel from the 90° detector bank.

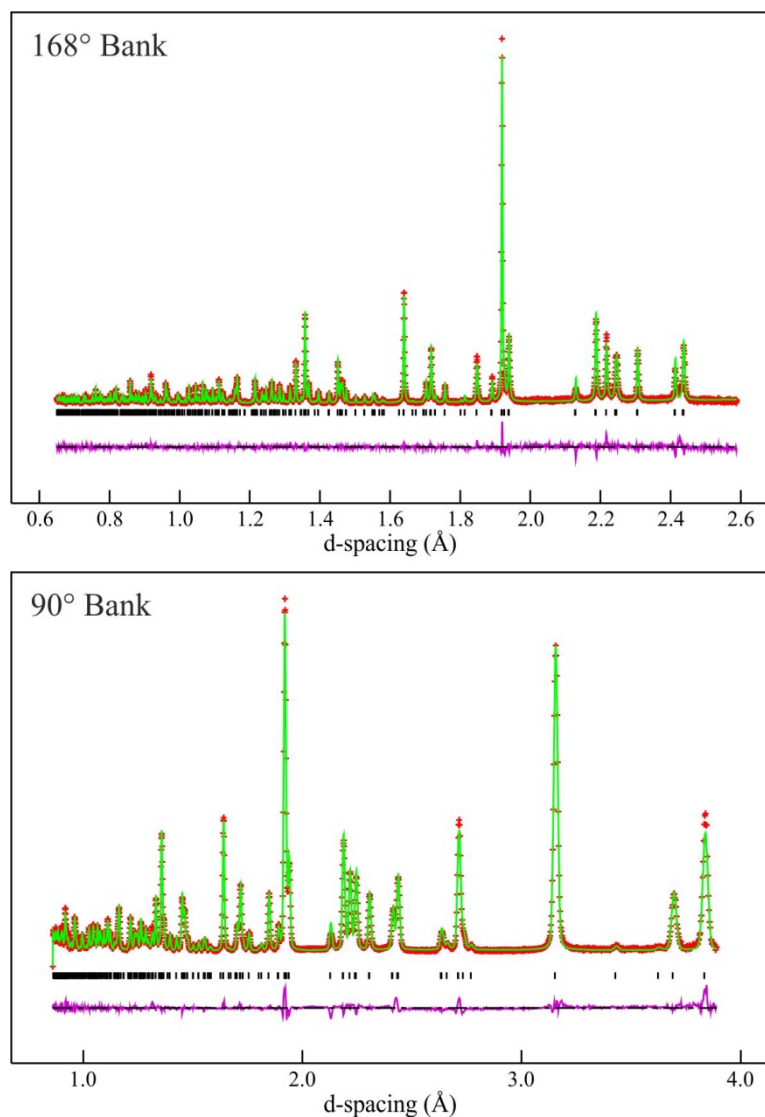


Figure S10. Observed, calculated and difference plots from the refinement of a structural model in space group *I2cm* (#46) against neutron powder diffraction data collected from RbNdTa₂O₇ at 298 K. Top panel shows data from the 168° detector bank, bottom panel from the 90° detector bank.

Atom	site	<i>x</i>	<i>y</i>	<i>z</i>	U _{iso} (Å ³)
Rb(1)	4 <i>a</i>	0.7521(12)	0	0	0.0364(4)
Nd(1)	4 <i>b</i>	0.7541(10)	0.9995(4)	¼	0.0105(3)
Nb(1)	8 <i>c</i>	0.2454(6)	0.0009(3)	0.35323(5)	0.0124(3)
O(1)	8 <i>c</i>	0.9943(7)	0.7597(8)	0.32438(8)	0.0197(4)
O(2)	8 <i>c</i>	0.0700(5)	0.2975(5)	0.34909(10)	0.0238(5)
O(3)	8 <i>c</i>	0.7447(9)	0.5527(4)	0.43222(8)	0.0218(5)
O(4)	4 <i>b</i>	0.7192(8)	0.4269(5)	¼	0.0176(9)
RbNdNb ₂ O ₇ – space group I2cm (#46) <i>a</i> = 5.4414(1) Å, <i>b</i> = 5.4278(1) Å, <i>c</i> = 21.9625(4) Å, volume = 648.65(4) Å ³ Formula weight: 527.51 g mol ⁻¹ , Z = 4 Radiation source: Neutron Time of flight Temperature: 298 K χ^2 = 8.23, wRp = 6.31%, Rp = 6.25%					

Table S4. Parameters from the structural refinement of RbNdNb₂O₇ against neutron powder diffraction data collected at 298 K.

Atom	site	<i>x</i>	<i>y</i>	<i>z</i>	U _{iso} (Å ³)
Cs(1)	2 <i>b</i>	0.2556(9)	0.2358(6)	½	0.0136(3)
Nd(1)	2 <i>a</i>	0.2740(5)	0.2456(3)	0	0.0033(3)
Ta(1)	4 <i>c</i>	0.7493(4)	0.2521(3)	0.1997(1)	0.0050(3)
O(1)	4 <i>c</i>	0.5128(6)	0.5184(6)	0.1447(1)	0.0126(4)
O(2)	4 <i>c</i>	0.9509(5)	0.9551(5)	0.1835(1)	0.0140(5)
O(3)	4 <i>c</i>	0.7511(6)	0.2926(3)	0.3563(1)	0.0118(4)
O(4)	2 <i>a</i>	0.7318(9)	0.1841(4)	0	0.0095(6)
CsNdTa ₂ O ₇ – space group P21am (#26) <i>a</i> = 5.4588(1) Å, <i>b</i> = 5.4494(1) Å, <i>c</i> = 11.2754(2) Å, volume = 335.41(1) Å ³ Formula weight: 751.03 g mol ⁻¹ , Z = 2 Radiation source: Neutron Time of flight Temperature: 298 K χ^2 = 5.63, wRp = 4.8%, Rp = 5.2%					

Table S5. Parameters from the structural refinement of CsNdTa₂O₇ against neutron powder diffraction data collected at 298 K.

Atom	site	<i>x</i>	<i>y</i>	<i>z</i>	U _{iso} (Å ³)
Rb(1)	4 <i>a</i>	0.7387(7)	0	0	0.0318(3)
Nd(1)	4 <i>b</i>	0.7279(5)	0.0034(3)	¼	0.0071(3)
Ta(1)	8 <i>c</i>	0.2491(4)	0.9993(3)	0.35261(3)	0.0044(2)
O(1)	8 <i>c</i>	0.9851(5)	0.7710(5)	0.32396(6)	0.0142(3)
O(2)	8 <i>c</i>	0.0590(4)	0.2938(5)	0.34500(7)	0.0175(4)
O(3)	8 <i>c</i>	0.7457(6)	0.5492(3)	0.43198(5)	0.0163(3)
O(4)	4 <i>b</i>	0.7697(8)	0.4318(4)	¼	0.0144(6)
RbNdTa ₂ O ₇ – space group I2cm (#46) <i>a</i> = 5.4305(1) Å, <i>b</i> = 5.4241(1) Å, <i>c</i> = 22.1683(3) Å, volume = 652.98(3) Å ³ Formula weight: 703.59 g mol ⁻¹ , Z = 4 Radiation source: Neutron Time of flight Temperature: 298 K χ^2 = 8.33, wRp = 4.85%, Rp = 4.96%					

Table S6. Parameters from the structural refinement of RbNdTa₂O₇ against neutron powder diffraction data collected at 298 K.

Cation	Anion	length (Å)	BVS
Rb(1)	O(3) × 2	2.848(2)	Rb +0.912
	O(3) × 2	3.079(8)	
	O(3) × 2	3.150(8)	
	O(3) × 2	3.349(2)	
Nd(1)	O(1) × 2	2.464(5)	Nd +2.99
	O(1) × 2	2.578(5)	
	O(2) × 2	2.637(3)	
	O(2) × 2	3.210(4)	
	O(4)	2.328(4)	
	O(4)	2.562(7)	
	O(4)	2.938(7)	
	O(4)	3.114(3)	
Nb(1)	O(1)	1.996(5)	Nb +5.05
	O(1)	2.058(5)	
	O(2)	1.874(4)	
	O(2)	2.080(4)	
	O(3)	1.759(2)	
	O(4)	2.305(1)	

Table S7. Selected bond lengths from the refined structure of RbNdNb₂O₇

Cation	Anion	length (Å)	BVS
Cs(1)	O(3) × 2	3.038(4)	Cs +1.06
	O(3) × 2	3.168(5)	
	O(3) × 2	3.210(5)	
	O(3) × 2	3.304(4)	
Nd(1)	O(1) × 2	2.520(4)	Nb +3.07
	O(1) × 2	2.533(2)	
	O(2) × 2	2.564(4)	
	O(2) × 2	3.147(3)	
	O(4)	2.354(4)	
	O(4)	2.521(6)	
	O(4)	2.979(6)	
	O(4)	3.115(3)	
Ta(1)	O(1)	2.004(4)	Ta +5.06
	O(1)	2.039(4)	
	O(2)	1.966(3)	
	O(2)	1.990(3)	
	O(3)	1.779(2)	
	O(4)	2.285(1)	

Table S8. Selected bond lengths from the refined structure of CsNdTa₂O₇

Cation	Anion	length (Å)	BVS
Rb(1)	O(3) × 2	2.873(2)	Rb + 0.88
	O(3) × 2	3.084(5)	
	O(3) × 2	3.150(5)	
	O(3) × 2	3.339(2)	
Nd(1)	O(1) × 2	2.496(3)	Nd +3.09
	O(1) × 2	2.577(3)	
	O(2) × 2	2.547(2)	
	O(2) × 2	3.186(3)	
	O(4)	2.335(3)	
	O(4)	2.513(5)	
	O(4)	2.963(4)	
	O(4)	3.109(3)	
Ta(1)	O(1)	1.998(3)	Ta +5.10
	O(1)	2.048(3)	
	O(2)	1.909(3)	
	O(2)	2.030(£)	
	O(3)	1.779(1)	
	O(4)	2.308(1)	

Table S9. Selected bond lengths from the refined structure of RbNdTa₂O₇